Design and control of a bidirectional wireless charging system using GaN devices

Haimeng Wu
School of Engineering
Newcastle University
Newcastle upon tyne, UK
Haimeng.Wu@newcastle.ac.uk

Bowen Gu
School of Engineering
Newcastle University
Newcastle upon tyne UK
b.gu2@newcastle.ac.uk

Xiang Wang
School of Engineering
Newcastle University
Newcastle upon tyne UK
x.wang108@newcastle.ac.uk

Volker Pickert
School of Engineering
Newcastle University
Newcastle upon tyne, UK
Volker.pickert@newcastle.ac.uk

Bing Ji
Department of Engineering
University of Leicester
Leicester, UK
Bing.ji@le.ac.uk

***Abstract*— Most of the existing wireless power transfer system works in unidirectional with one-direction control signals. This paper presents a bidirectional wireless charging system with a duplex communication method, which is not only able to achieve the two-way wireless power transmission, but also transfers control signals bi-directionally. The power circuit operation mode is actively controlled by using the wireless transceiver module which can duplex communication to deliver measured signals remotely. The operational principle is analytically studied in details and is verified by simulation. Finally, a prototype of the bidirectional charging system using GaN devices has been successfully designed and tested. In addition, the measured feedback signals are effectively transmitted to validate the control algorithm.**

Keywords—wireless power transfer system, bidirectional, duplex communication, GaN devices

I. INTRODUCTION

Wireless power transfer (WPT) technology has been developing rapidly in industry which is able to provide a reliable, flexible and cost-efficient power delivery solution. Particularly, in many environments that are hindered by the wired connection, this technique shows huge potential such as home appliances, medical applications and the most concerned field – electric vehicles [1]-[3]. The most mature technique used in WPT is electromagnetic induction, there are numerous literatures focused on this technique handling with how to improve transmit efficiency and specially looking into the contribution based on the study of different topologies [4] - [7]. The widely used topologies by manufactures are SS (series-series), LCL and LCC compensation. In this field, most research is concerned with one-way transmission system. However, with the increasing demand on the convenient power energy sharing, the bidirectional WPT technique shows the great superiority and needs to be further developed. In addition, the development of the next generation wide bandgap device such as gallium nitride (GaN) power semiconductors provides the opportunity to achieve the high power conversion with higher power density and lower losses [8].

Regarding the communication of wireless power transfer, the amplitude shift key (ASK) technique and frequency shift key (FSK) techniques are most commonly used methods which are presented in many publications [9] - [11]. However, some issues has been reported such as low power efficiency, susceptible to noise interference for ASK and larger bandwidth are required for FSK. Fundamentally, however, both of the techniques lack of the capability of duplex communication and transmission of diverse information [12]. In addition, another method of using extra coils with multiple carriers is proposed in [13]. The main issue of this technique is the large noise generated from the strong power signal to small data signal. With the fast development of wireless communication technique, a great number of low cost, high performance transceivers modules are available on the market. In this paper, a bidirectional wireless charging system using GaN devices have been developed based on SS structure with a proposed duplex communication method for bidirectional close loop control. A cost-effective wireless communication module nRF24L01+ has been applied for the data transmit during power transfer in order to achieve the proposed control strategy [14].

II. THEORETICAL PRINCIPLE

The diagram of the proposed bidirectional WPT circuit is presented in Fig. 1. One side of the converter is composed of a full active bridge with LC resonator; the other side of the converter consists of LC resonator, a full bridge and a bidirectional step up/down converter. The operational modes of this circuit are shown in the Fig.2 (a) and 2 (b). In the forward power transfer mode, the active bridges with four switches are operated in the primary side and four in body diodes are working with the bidirectional step up/down converter that operates as a buck converter. In the backward power transmission mode, the primary becomes a boost converter in series with a full active bridge, and the secondary is configured as the four diodes which operate as a rectifier.

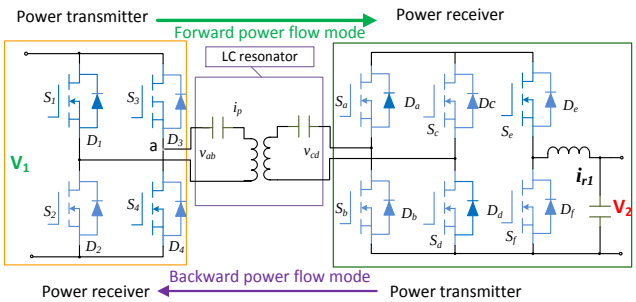

Figure 1 The proposed bidirectional WPT circuit

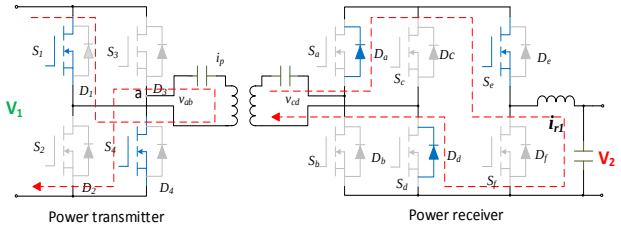

Figure 2 (a) Forward operation mode

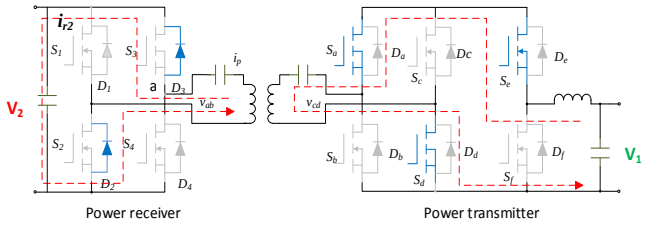

Figure 2 (b) Backward operation mode

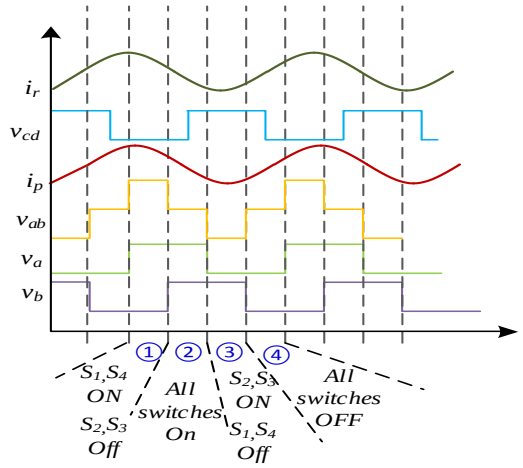

Figure 3 Key operational waveform of bidirectional WPT system

The phase shift control method is chosen for controlling the charging current to the load. The main concept of phase shift angle control is to control the switching timing of different bridge arms while ensuring that the two switches of the same bridge are complementary in timing. The key operational waveform using the phase shift control method in the forward mode is presented in Fig.3.

The wireless transmission section of the proposed topology is based on the SS structure which is able to achieve the highest transmission power in the short distance, compared to the other types of structure. The basic schematic of SS topology is shown in Fig.4 (a) and Fig.4 (b) shows the equivalent circuit of the proposed circuit that includes the SS topology and the bidirectional step up/down converter.

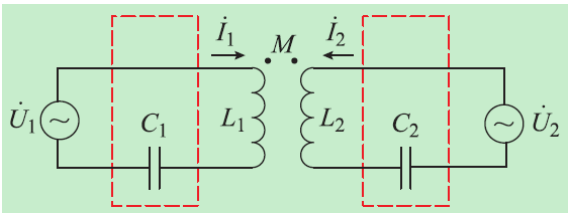

Figure 4 (a) Simplified circuit of SS topology

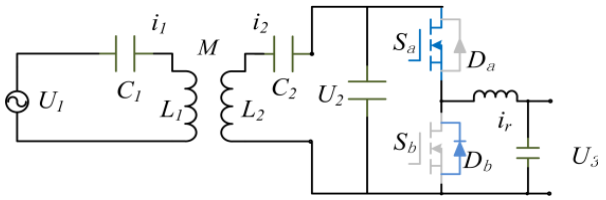

Figure 4 (b) SS topology assembly with step-down circuit

Under the condition of fully resonate, the below equation can be derived:

$$\omega = \frac{1}{\sqrt{L_1 C_1}} = \frac{1}{\sqrt{L_2 C_2}} \tag{2.1}$$

According to the Fourier transform equation:

$$a_n = \frac{2}{T}\int_{x}^{x+T} f(x)\cdot\cos(\frac{2\pi nx}{T})dx \tag{2.2}$$

$$b_n = \frac{2}{T}\int_{x}^{x+T} f(x)\cdot\sin(\frac{2\pi nx}{T})dx \tag{2.3}$$

Where n is the order of the harmonics and T is the period of the output, Considering the fully resonate condition, only the fundamental frequency is concerned in this case and select the output waveform as sinusoidal type:

$$a_1 = 0 \tag{2.4}$$

$$b_1 = \frac{8V_1}{\omega p}\sin(\frac{\varphi}{2}) \tag{2.5}$$

Where V_1 is the input DC bus voltage of the primary side, φ represents the phase angle of legs from the primary side inverter. Based on equation (2.4) and (2.5), the primary side output voltage and the charging current can be derived:

$$U_p = f(V_1,\varphi) = \frac{2\sqrt{2}V_1}{\pi}\sqrt{1-\cos\varphi}\cdot\sin\omega t \tag{2.6}$$

$$i_{r1} = \frac{1}{D_1}\cdot\frac{1}{\sqrt{2}}\cdot\left|I_2\right| \tag{2.7}$$

Where D_1 is the duty ratio of the switch from buck converter and i_{r1} is the charging current. Also, the KVL equation of both sides based on Fig.4 (a) are shown below:

$$U_p = \left(j\omega L_1 + \frac{1}{j\omega C_1}\right)I_1 + j\omega I_2 M = j\omega I_2 M \tag{2.8}$$

$$U_s = \left(j\omega L_2 + \frac{1}{j\omega C_2}\right)I_2 + j\omega I_1 M = j\omega I_1 M \tag{2.9}$$

Where M is the mutual inductance, I_1 and I_2 are the primary side current and secondary side current respectively. In principle, the converter based on the SS structure is a voltage controlled current source for the load.

Substituting equation (2.1), (2.4) and (2.5) into (2.7), the following charging current i_{r1} under forwarding operation mode can be obtained:

$$i_{r1} = f(V_1, \varphi, D_1) = \frac{1}{D_1} \cdot \frac{2V_1}{\omega M \pi} \sqrt{1-\cos\varphi} \qquad (2.10)$$

Similarly, the equation of backward operation mode can be obtained based on the same KVL equation (2.8) and (2.9). In this case, the output voltage of primary side and charging current of the load can be derived:

$$\dot{U}_p = f(V_1, \varphi, D_2) = \frac{1}{1-D_2} \cdot \frac{2\sqrt{2}V_2}{\pi} \sqrt{1-\cos\varphi} \cdot \sin\omega t \qquad (2.11)$$

$$i_{r2} = \frac{1}{\sqrt{2}} \cdot \left| \dot{I}_2 \right| \qquad (2.12)$$

Substituting the equation (2.7), (2.4) and (2.5) into (2.8), the charging current under backward mode can be obtained:

$$i_{r2} = f(V_1, \varphi, D_2) = \frac{1}{1-D_2} \cdot \frac{2V_2}{\pi\omega M} \sqrt{1-\cos\varphi} \qquad (2.13)$$

Where D_2 is the duty ratio of the switch of the boost converter and V_1 is the input voltage of the boost converter. As can be seen, the charging current can be achieved by adjusting the phase angle with fixed duty ratio D_2. And constant output power can be accomplished with the benefit of the equivalent circuit regardless the resistive or capacitive load.

III. SIMULATION VERIFICATION

In order to develop the advanced control algorithm, the influence of coil distance on mutual inductance is investigated in the finite element software Maxwell. Fig. 5 shows the electromagnetism result of the coil model which consists of two round coils on the square ferrite opposite with each other.

The 2A excitation current is injected into the coil and the distance between the coils ranges from 1mm to 50mm for different power transfer condition. Table 1 lists the simulation results between self-inductance and coupling coefficient among different distance. It clearly shows that the coupling coefficient decreases while the distance increases. Also, once the distance between two coils is beyond 50mm, the coupling coefficient is too small that may introduce failure to the circuit.

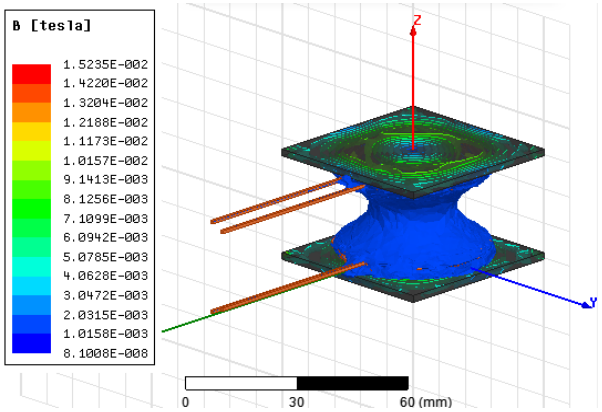

Figure 5 ANSYS Maxwell simulation results among different distance

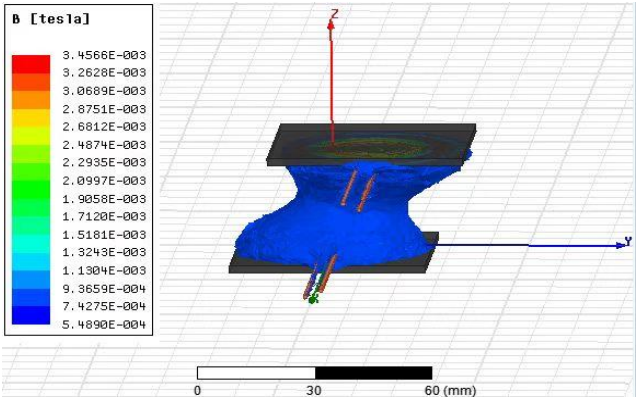

Figure 6 ANSYS Maxwell simulation results misaligned position (Y-axis offset 10mm)

Table 1 Simulation results under different distance

Distance (mm)	1	5	10	20	50
Self-inductance/μH	11.10	9.50	8.82	8.50	8.43
Coupling coefficient	0.761	0.540	0.343	0.145	0.018

Table 2 Simulation results under different relative position

Y-axis offset (mm)	-30	-10	0	10	30
Self-inductance/μH	8.672	8.673	8.688	8.672	8.671
Coupling coefficient	0.016	0.122	0.149	0.122	0.016

Table 3 Specification of the simulation in Matlab/Simulink

Parameters	Values	Parameters	Values
Input V_1(V)	14.2	Phase	0-180°
Output V_2(V)	7.1	Current I_r (A)	0-2A
Frequency(kHz)	500	Coupling factor	0.2
C_{r1}, C_{r2} (nF)	10	L_{r1}, L_{r2} (μH)	10

In practical applications, the placement of the coils cannot always been aligned. In order to investigate the influence of the misaligned position of the coils to the coupling coefficient, another simulation is carried out. Fig. 6 illustrates one case of the simulation results on misaligned position when the Y-axis offset is 10mm. Table 2 presents the simulation results between self-inductance and coupling coefficient among different misaligned position based on the Z-axis distance at 20 mm. It can be seen that the aligned position has the maximum coupling coefficient and with the misaligned position increases, the coupling coefficient decreases dramatically.

Table 3 lists the specification of the parameters used in Matlab/Simulink. Fig.7 (a) presents the proposed circuit built in the simulation tool and the key operational waveform which consists of the voltage and current of the resonant network in both of the primary and secondary is shown in Fig.7 (b). As can be seen, with the phase angle increases from 90° to 180°, the secondary charging current is increasing from 1.4A to 2A, which is consist with the theoretical analysis in section II.

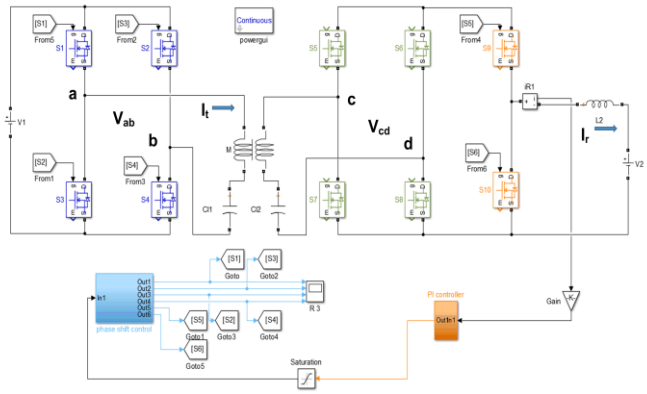

Figure 7 (a) The simulation circuit in Matlab/Simulink

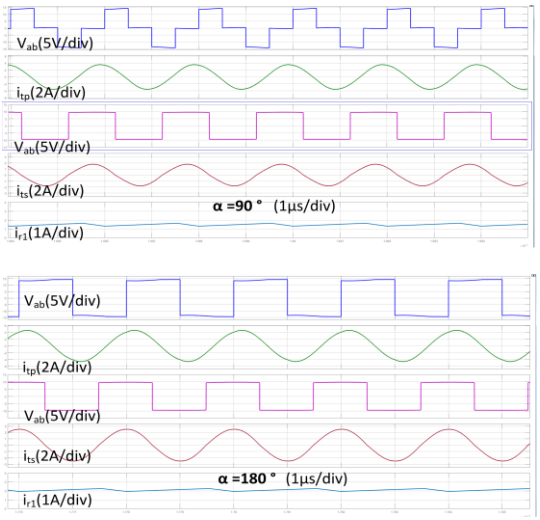

Figure 7 (b) Key operational waveforms

IV. EXPERIMENTAL VALIDATION

The prototype photograph of the developed bidirectional wireless power converter is shown in Fig.8 (a) which has been placed in an enclosure with the periphery protection circuit and the digital volt-amp meters for the battery voltage and current display. By processing the measured command signal, the charging current and power transfer direction can be manually controlled by the external turning button and switches. The configuration of the proposed bidirectional wireless charging system is shown in Fig.8 (b).

Table 4 Specification of the prototype

Parameters	Values	Parameters	Values
L_{r1}, L_{r2} (μH)	10	C_{r1}, C_{r2} (nF)	10
Frequency(kHz)	500	Coupling factor	0.2
Devices	Type	Devices	Type
Rechargeable Lion battery V1	14.8V 5600mAh	Rechargeable Lion battery V2	7.4V 5600mAh
Transceiver module	nRF24L01+	GaN power switch	EPC 2021

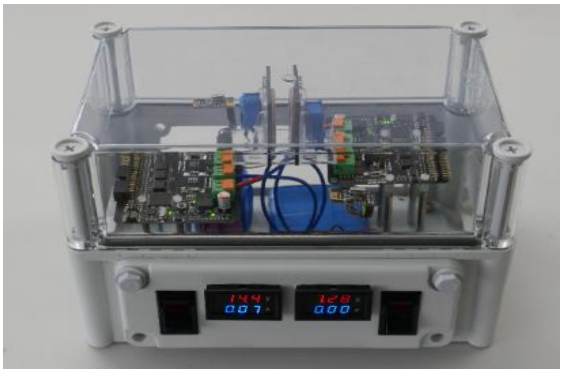

Figure 8 (a) The prototype of the converter

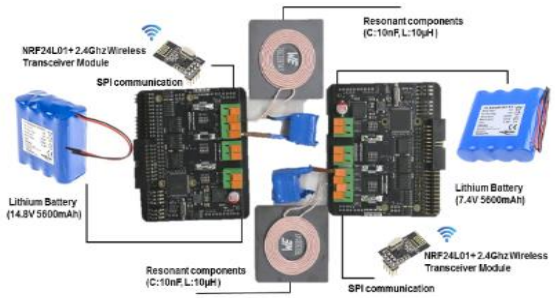

Figure 8 (b) The configuration of the WPT system

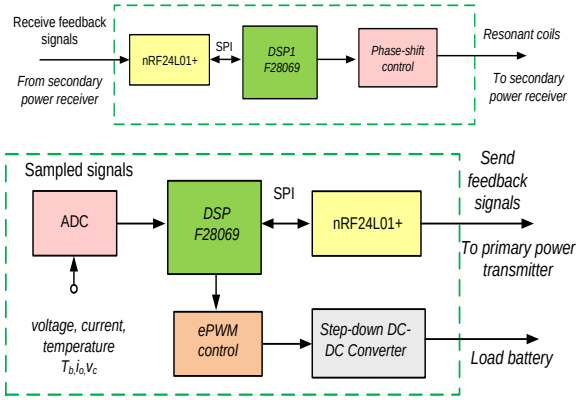

Figure 9 Control algorithm in the power transmitter and power receiver

The specification of the prototype is chosen based on the parameters of simulation model. GaN power switched are applied to achieve the high power conversion. Table 4 lists the specification of the prototype and the selected devices.

Fig.9 illustrates the control algorithm in both the power transmitter and power receiver. Instead of using conventional ASK or FSK techniques for only unidirectional communication signals, a duplex communication method by using the wireless transceiver modules is proposed for the bidirectional close loop control. When the circuit is configured as the power receiver, is becomes the signal transmitter since the measured signals such as voltages, current, and temperature from the circuit should be transferred into the wireless transceiver modules through the SPI communication and then they are sent to the power transmitter which is also known as the signal receiver. The controller of power transmitter receives the signals from the transceiver module and then processes them to adjust the phase shift angle which can control the charging current at the power receiver side.

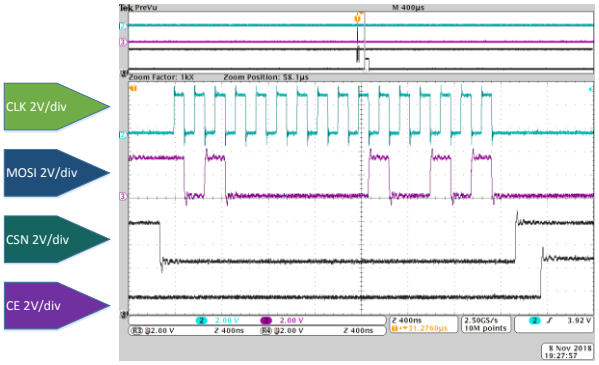

Figure 10 (a) SPI wireless communication waveforms of power receiver/ signal transmitter

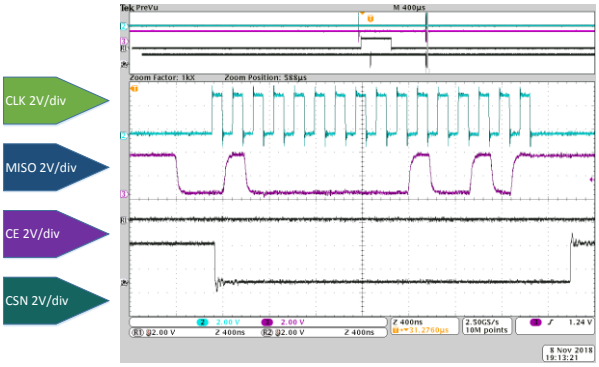

Figure 10 (b) SPI wireless communication waveforms of power transmitter/ signal receiver

Fig.10 (a) shows the SPI wireless communication waveforms between the transceiver module and the DSP from the power receiver side. From the top to bottom are clock signal (CLK), command /data signal from DSP to nRF through SPI communication (MOSI), Chip selection signal (CSN) and Enabling signal (CE) respectively. Similarly, Fig.10 (b) shows the SPI wireless communication waveforms between the transceiver module and the DSP from the power transmitter side. From the top to bottom are clock signal (CLK), command /data signal from nRF to DSP through SPI communication (MISO), Chip selection signal (CSN) and Enabling signal (CE) respectively. According to the mechanism of the transceiver, the transmitted and the received command and data signal are generated at the first and last 8 bits CLK respectively. It can be seen that the value of 0x25 in binary received in Fig. 10 (b) which is the same as the transmitted signal shown in Fig.10 (a). Therefore, the results confirm that the successful communication between the two sides, which is the basis of achieving the wireless close loop control.

The experimental results by applying the proposed closed loop control strategy are shown below, the bidirectional wireless power transfer has been achieved by either utilizing the external commands or the internal negotiated communication mechanisms. These waveforms are recorded at different pre-set reference values. From the top to the bottom are primary voltage, secondary current, secondary voltage and primary current respectively. As can be seen that from Fig.11 (a) to (c) the reference charging current increases by manually changing the external tuning switch. Therefore, the secondary current rises accordingly with the primary output voltage stays at peak value for longer period which validates the theoretical principle and the simulation

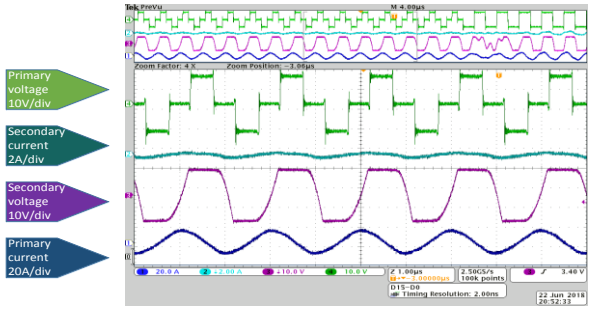

Figure 11 (b) Closed loop key operational waveforms of 90°

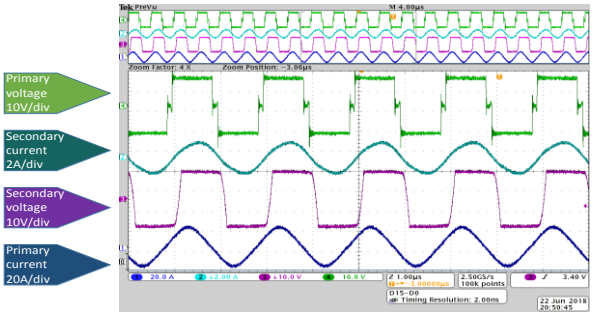

Figure 11 (b) Closed loop key operational waveforms of 170°

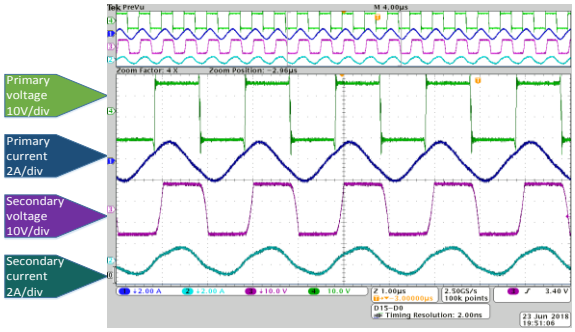

Figure 11 (c) Closed loop key operational waveforms of 180°

results. The peak output power can be achieved around 28W with adjusting the phase angle at the top value.

In addition, there are differences of the secondary current value between the simulation results and the experimental tests from the below waveforms. The possible reason of this phenomenon is the measured current from the experiment is the DC-bus current and the measured current in simulation is from the step-down DC-DC converter. But the trend from the both waveforms stays the same.

V. CONCLUSION

A bidirectional wireless charging system using GaN devices is presented in this paper. The operational modes of the proposed circuit are studied with the given theoretical analysis. The simulation reveals the relationship of the distance between the resonant coil and the coupling coefficient which is relevant to the transmission efficiency. In addition, the influence between the coupling coefficient and the relative position is carried out. A control algorithm is proposed that applies wireless transceiver to achieve the communication between the power transmitter and receiver. The experimental results successfully prove the theoretical principle and validate the bidirectional power transfer and duplex communication.

REFERENCES

[1] H. Wu, V. Pickert, S. Lambert, P. Allanf, X. Deng and H. Zhan, "A ripple reduction method for a two stages battery charger with multi-winding transformer using notch filter," *2017 IEEE 12th International Conference on Power Electronics and Drive Systems (PEDS)*, Honolulu, HI, 2017, pp. 1,101-1,106.

[2] S. Zhou and C. Chris Mi, "Multi-Paralleled LCC Reactive Power Compensation Networks and Their Tuning Method for Electric Vehicle Dynamic Wireless Charging," in *IEEE Transactions on Industrial Electronics*, vol. 63, no. 10, pp. 6546-6556, Oct. 2016.

[3] H. Wu, V. Pickert, X. Deng, D. Giaouris, W. Li and X. He, "Polynomial Curve Slope Compensation for Peak-Current-Mode-Controlled Power Converters," in *IEEE Transactions on Industrial Electronics*, vol. 66, no. 1, pp. 470-481, Jan. 2019.

[4] Y. Zhang, K. Chen, F. He, Z. Zhao, T. Lu and L. Yuan, "Closed-Form Oriented Modeling and Analysis of Wireless Power Transfer System With Constant-Voltage Source and Load," in IEEE Transactions on Power Electronics, vol. 31, no. 5, pp. 3472-3481, May 2016.

[5] K. Chen, Z. Zhao, F. Liu, L. Yuan, "Resonance Topology Analysis of Two-way Wireless Charging System for Electric Vehicles," in AEPS, vol. 41, no. 2, Jan 2017.

[6] H. Feng, T. Cai, S. Duan, J. Zhao, X. Zhang and C. Chen, "An LCC-Compensated Resonant Converter Optimized for Robust Reaction to Large Coupling Variation in Dynamic Wireless Power Transfer," in IEEE Transactions on Industrial Electronics, vol. 63, no. 10, pp. 6591-6601, Oct. 2016.

[7] W. Li, H. Zhao, J. Deng, S. Li and C. C. Mi, "Comparison Study on SS and Double-Sided LCC Compensation Topologies for EV/PHEV Wireless Chargers," in IEEE Transactions on Vehicular Technology, vol. 65, no. 6, pp. 4429-4439, June 2016.

[8] E. A. Jones, F. F. Wang and D. Costinett, "Review of Commercial GaN Power Devices and GaN-Based Converter Design Challenges," in IEEE Journal of Emerging and Selected Topics in Power Electronics, vol. 4, no. 3, pp. 707-719, Sept. 2016.

[9] Chen-Hua Kao and Kea-Tiong Tang, "Wireless power and data transmission with ASK demodulator and power regulator for a biomedical implantable SOC," 2009 IEEE/NIH Life Science Systems and Applications Workshop, Bethesda, MD, 2009, pp. 179-182.

[10] A. Yakovlev, S. Kim and A. Poon, "Implantable biomedical devices: Wireless powering and communication," in IEEE Communications Magazine, vol. 50, no. 4, pp. 152-159, April 2012.

[11] W. P. Choi, W. C. Ho, X. Liu and S. Y. R. Hui, "Bidirectional communication techniques for wireless battery charging systems & portable consumer electronics," 2010 Twenty-Fifth Annual IEEE Applied Power Electronics Conference and Exposition (APEC), Palm Springs, CA, 2010, pp. 2251-2257.

[12] X. Lu, P. Wang, D. Niyato, D. I. Kim and Z. Han, "Wireless Charging Technologies: Fundamentals, Standards, and Network Applications," in IEEE Communications Surveys & Tutorials, vol. 18, no. 2, pp. 1413-1452, Second quarter 2016.

[13] U. K. Madawala, J. Stichbury, and S. Walker, "Contactless power transfer with two-way communication," in proc. IEEE Conf. Ind. Electron., Busan, Korea, Nov. 2004, pp. 3071-3075.

[14] "SDI TAPAS - Community Inverter - Quick-Start Guide", 2018.